THERMODYNAMIC MODELING OF SUSTAINABLE NON-FERROUS METALS PRODUCTION

Phase Equilibrium Study of the CaO-SiO$_2$-MgO-Al$_2$O$_3$-TiO$_2$ System at 1300°C and 1400°C in Air

JUNJIE SHI,[1,2] MIN CHEN,[1,3] XINGBANG WAN,[1,4] PEKKA TASKINEN,[1,5] and ARI JOKILAAKSO[1,6]

1.—Department of Chemical and Metallurgical Engineering, School of Chemical Engineering, Aalto University, Kemistintie 1F, P.O. Box 16100, 00076 Aalto, Finland. 2.—e-mail: junjieshi@126.com. 3.—e-mail: min.chen@aalto.fi. 4.—e-mail: xingbang.wan@aalto.fi. 5.—e-mail: pekka.taskinen@aalto.fi. 6.—e-mail: ari.jokilaakso@aalto.fi

Due to the importance of the physicochemical properties of slag in the recovery of low-titanium ores and by-products, the equilibrium phase relationships of the CaO-MgO-Al$_2$O$_3$-SiO$_2$-TiO$_2$ system were experimentally determined using a high-temperature equilibration and quenching method at 1300°C and 1400°C. The equilibrium information was obtained by scanning electron microscope–energy dispersive x-ray spectrometer. Perovskite, spinel and pseudobrookite solid solution phases with MgO·2TiO$_2$ and Al$_2$O$_3$·TiO$_2$ end members were found to be coexisting with the liquid phase. The 1300°C and 1400°C isotherms were then constructed on a CaO-SiO$_2$-TiO$_2$-8 wt.% MgO-14 wt.% Al$_2$O$_3$ quasi-ternary section. Comparisons with predictions by Factsage and MTDATA indicated that the computational results agreed well only in the primary phase field of perovskite, while clear deviations existed within other primary phase fields. Therefore, the present results improve our knowledge about the utilization of titanium resources, and are also significant in providing novel equilibrium data for updating the related thermodynamic databases.

INTRODUCTION

Nowadays, energy conservation and environmental emissions[1] have become a serious challenge for the modern metallurgical industry, necessitating, for example, lower coke consumption and greenhouse gas emissions.[2] To meet these important criteria, systematic research on both fundamental theory and equipment is essential. It is well known that the physicochemical properties of slag phases, including viscosity,[3] surface tension,[4,5] liquidus,[6] and phase relationships,[7] have a great effect on product quality in iron and steelmaking. Therefore, it is necessary to optimize the key physicochemical properties of the slag phase, where the equilibrium phase relationships and liquidus contour information have the highest priority.

Current iron and steelmaking slags can be basically described using the CaO-MgO-Al$_2$O$_3$-SiO$_2$ system, which has been extensively investigated[8–11] during recent decades. The resulting phase diagrams have been collected in compilations such as the Slag Atlas.[12] The abundant phase diagram information of the CaO-MgO-Al$_2$O$_3$-SiO$_2$ system can act as a key reference for further studies of the equilibrium phase relationships and liquidus equilibria influenced by further additions of oxides, including Cr$_2$O$_3$,[13] MnO,[14] FeO [15] and TiO$_2$.[16] During smelting of titano-magnetite ores, a titanium-bearing slag is produced as a by-product, which can be described as the CaO-MgO-Al$_2$O$_3$-SiO$_2$-TiO$_2$ quinary system.[17] Therefore, accurate phase equilibrium data regarding the quinary system are greatly needed for a smooth operation of the titano-magnetite smelting reduction process.

However, the equilibrium phase relationships for this quinary system have not yet been fully explored. The first systematic investigation of the CaO-MgO-Al$_2$O$_3$-SiO$_2$-TiO$_2$ system was conducted by Osborn et al.[18] for TiO$_2$ contents varying from 2.5 wt.% to 10 wt.% in air. The results were plotted in quasi-ternary phase diagrams with fixed contents of Al$_2$O$_3$ (10 wt.%, 15 wt.%) and TiO$_2$ (2.5 wt.%, 5 wt.%, 10 wt.%). Later, Shi et al.[19–21] conducted a

series of static and dynamic experiments in air on the equilibrium phase relationships and liquidus for a Ti-bearing slag system within the range of 2.5 wt.% to 25 wt.% TiO$_2$ with fixed MgO (5 wt.%) and Al$_2$O$_3$ (10 wt.%, 20 wt.%, 30 wt.%) contents. Zhao et al.[22] carried out equilibrium studies in reducing conditions at carbon saturation, and the obtained results were mainly projected with constant $w(MgO)/w(CaO)$ ratios of 0.20–0.72 and $w(Al_2O_3)/w(SiO_2)$ of 0.4–0.6. Later, Wang et al.[23] studied the equilibrium phase relationships at carbon saturation with 10 wt.% Al$_2$O$_3$ and 5 wt.% MgO. They focused on TiO$_2$ contents higher than 40 wt.%, with the aim of finding the optimum composition range for the anosovite solid solution used for selective crystallization and separation of TiO$_x$. Nowadays, many thermodynamic databases have been established and successfully used for phase diagram predictions in oxide systems, for example, CaO-SiO$_2$,[24] CaO-Al$_2$O$_3$-SiO$_2$,[25] CaO-TiO$_2$,[26] and CaO-MgO-SiO$_2$-TiO$_2$[27] systems. However, the calculated phase diagrams for higher order systems are still far from accurate, as pointed out by Wang et al.,[28] who reported that errors in the liquidus temperature calculated by Factsage may reach + 130°C in the primary phase field of TiO$_2$. Therefore, it can be concluded that the available studies on the equilibrium phase relationships of the TiO$_2$-containing quinary system were quite inadequate from both experimental and modeling perspectives.

The equilibrium phase relationships for the CaO-MgO-Al$_2$O$_3$-SiO$_2$-TiO$_2$ system, directly related to the industrial composition range of titanium-bearing slags, were experimentally investigated in the present work by the high-temperature equilibration and quenching method. The experimental results were compared with predictions by thermodynamic software programs Factsage and MTDATA using their database.[29,30] It is evident that the present experimental results will not only offer a fundamental understanding of the smelting process of magnetite ore but also provide basic thermodynamic data to be used in the solution parameter optimization of databases for titanium-bearing oxide systems.

EXPERIMENTAL

The experimental techniques and set-up have been presented earlier in the literature[31,32] and therefore only selected novel features will be presented in this paper.

Samples

The initial compositions of the samples were designed based on industrial compositions of Ti-bearing slags.[17,33,34] The 0.15-g mixture samples were prepared by accurately mixing (± 0.1 mg) high purity oxide powders of CaO (99.99 wt.%), SiO$_2$ (99.99 wt.%), MgO (99.995 wt.%), Al$_2$O$_3$ (99.99

wt.%), and TiO$_2$ (99.8 wt.%) from the suppliers Sigma-Aldrich or Alfa Aesar. The blend was thoroughly mixed, and then pressed into small cylinders and stored in a desiccator prior to use. In order to reflect the influence of the $w(CaO)/w(SiO_2)$ ratio and TiO$_2$ content on the equilibrium phase relationships, the MgO and Al$_2$O$_3$ contents were fixed during sample preparation at 10 wt.% and 15 wt.%, respectively.

Equilibrium Experiments

A vertical corundum tube furnace with an inner diameter of 40 mm was employed for the equilibrium experiments in air atmosphere, as shown in Fig. 1. Two thermocouples, regularly calibrated to an accuracy of ± 3°C, were used for monitoring the furnace temperature. The high-temperature equilibration and quenching method was employed in the experiments. During the experiments, the pressed sample was placed inside a platinum foil, suspended by a platinum wire in the center of the even temperature zone of the furnace, just next to the measurement thermocouple (see Fig. 1). The temperature was first increased to 50°C above the
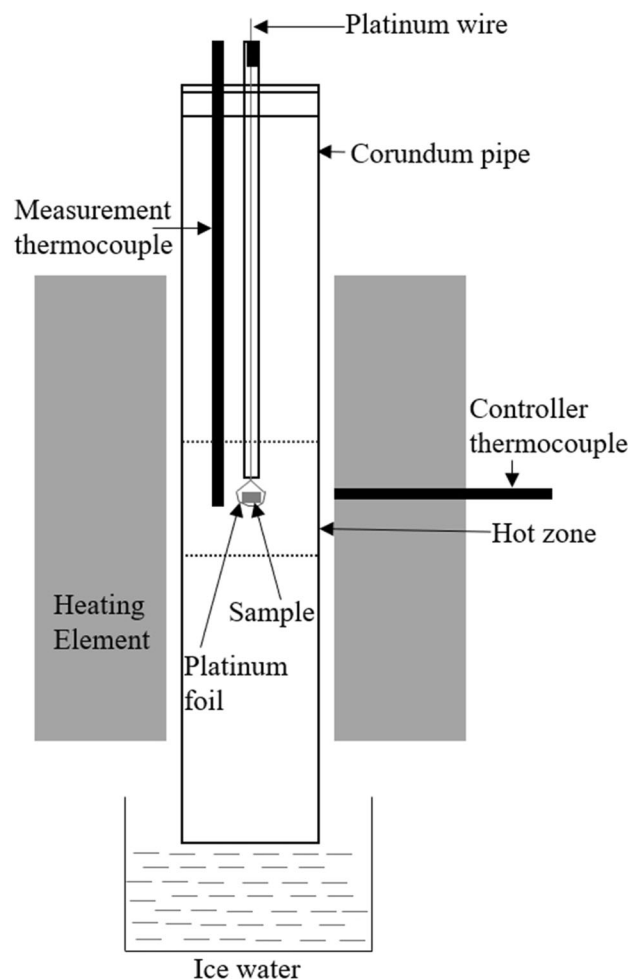

Fig. 1. Schematic of the vertical tube furnace.

equilibration temperature at least for 60 min to accelerate dissolution of the materials, and thereafter decreased to the equilibrium temperature (1300°C or 1400°C), which was maintained long enough to ensure equilibrium. Preliminary experiments with extended lead times of 720–2880 min proved that 1440 min was sufficient to reach equilibrium.[31] Therefore, each sample was equilibrated for at least 1440 min. After equilibration, the sample was dropped from the furnace into ice-water placed just below the reaction tube. The vertical position of the furnace allowed the quenching process to finish within seconds to retain the high-temperature phase assemblage at room temperature. The quenched sample was then dried and stored in the desiccator for phase analysis.

Analysis

The quenched sample was mounted in epoxy resin, polished, and coated with carbon. The phase assemblage and phase compositions were measured using a Tescan MIRA 3 Scanning Electron Microscope (SEM; Tescan, Brno, Czech Republic) equipped with an UltraDry Silicon Drift Energy Dispersive X-Ray Spectrometer and NSS Microanalysis Software (EDS; Thermo Fisher Scientific, Waltham, MA, USA). The following parameters were employed: an accelerating voltage of 15 kV, and a beam current of 20 nA. The Proza (Phi-Rho-Z) matrix correction procedure was used for raw data processing. The standards utilized in the EDS analyses were Al metal (for Al, $K\alpha$), calcite (for Ca, $K\alpha$), Mg metal (for Mg, $K\alpha$), olivine (for O, $K\alpha$), quartz (for Si, $K\alpha$), and Ti metal (for Ti, $K\alpha$). At least six analysis points were randomly selected from each phase for statistical reliability. As titanium can only exist as Ti^{4+} in air, the analyzed titanium will therefore be expressed as tetravalent TiO_2.

Thermodynamic Calculations

The present experimental results were compared with predictions by the thermodynamic software Factsage 7.3[35] and MTDATA 6.0.[36] For the Factsage predictions, the "FactPS" and "FToxid" databases were used in the Equilib module, and the oxygen partial pressure was set as 0.21 atm. The solution phases in Factsage were described by the quasi-chemical model,[29] and the solid phases retrieved were ilmenite, pseudobrookite, rutile, titania spinel and magneli phases. In the MTDATA predictions, the isothermal quasi-ternary liquidus contour sections for the Ti-bearing slag system were calculated using the Mtox database, v.8.1,[30] where a full assessment of the $CaO-Fe-Ti-O-MgO-Al_2O_3-SiO_2$ system was available. For the isothermal 1300°C and 1400°C sections calculated by MTDATA,[32] the stoichiometric and solution phases were as follows: stoichiometric phases of cordierite ($Al_4Mg_2Si_5O_{18}$) and sphene ($CaSiTiO_5$), and solid solution phases of

feldspar $((Al,Ca)(Al)Si_2O_8)$, melilite $((Al,Ca)_2(Ca,Mg)_2Si_2O_7)$, olivine $((Ca,Mg)(Ca,Mg)SiO_4)$, perovskite $((Ca)(Al,Ti)(O,Va)_3)$, pseudo-brookite $((Al,Mg,Ti)(Al,Mg,Ti)_2O_5)$, spinel[37] $((Al,Mg)(Al,Ca,Mg,Ti)_2(Mg,Va)_2O_4)$, and titanium(III)oxide $(((Mg,Ti)_{0.5},Ti)_2(Va)(O)_3)$, where Va is a vacancy in a sub-lattice.

RESULTS AND DISCUSSION

Equilibria Phase Relations at 1400°C

The phase morphologies and obtained compositions of the equilibrium phases at 1400°C are shown in Fig. 2 and Table I, respectively. Overall, the equilibrium assemblage at 1400°C was straightforward and only solid perovskite was found to coexist with the liquid oxide phase.

In Fig. 2a, the microstructure of the equilibrium phase for sample #2 is taken as an example to exhibit a single glassy phase after quenching, which means that sample #2 was located in the homogeneous liquid phase domain at 1400°C. In Fig. 2b, a two-phase equilibrium was found in sample #9 at 1400°C. In combination with the compositions given in Table I, it was easy to conclude that the white phase is perovskite, simplified as $CaO \cdot TiO_2$, while the gray matrix phase was the coexisting liquid oxide. Samples #6, #12, and #16 all demonstrated liquid–perovskite two-phase equilibria at 1400°C. This proves that the initial compositions of these samples were located within the primary phase field of perovskite. Therefore, the two-phase tie lines were projected and compared on a quasi-ternary phase triangle, as shown in Fig. 3a, which illustrates the progress of the equilibrium and liquidus line compositions as a function of silica concentration.

It is worth mentioning that, during preparation of the initial compositions, fixed levels of 10 wt.% and 15 wt.% were targeted for the MgO and Al_2O_3 contents, respectively. However, compositions of the equilibrium liquid oxide will hardly ever lie exactly on the 10 wt.% MgO and 15 wt.% Al_2O_3 planes due to the precipitation of solid phases (e.g., in this case, perovskite), or the weighting and mixing during the sample preparing process. Therefore, a recalculation is needed in most points. As can be seen in Table I, the analyzed MgO and Al_2O_3 contents in the liquid oxide were close to 8 wt.% and 14 wt.%, respectively. Thus, it was reasonable to project the liquid compositions onto the 8 wt.% MgO and 14 wt.% Al_2O_3 plane for presentation purposes. Normalization was carried out according to the following steps: the MgO and Al_2O_3 contents were first adjusted to 8 wt.% and 14 wt.%, respectively, while the sum of the three remaining oxides were adjusted to 78 wt.% using their original relative mass fraction ratios. The normalized composition could then be projected onto the quasi-ternary phase diagram.
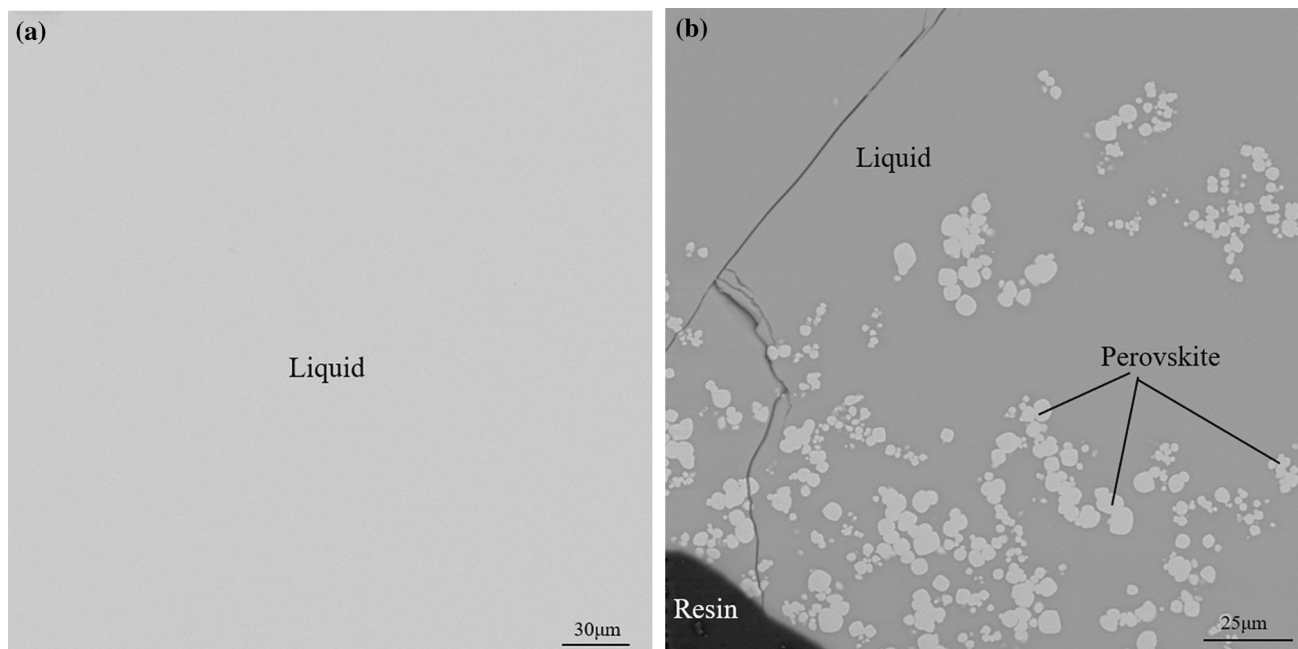
Fig. 2. SEM microscopic morphologies of the equilibrium phases at 1400°C. (a) #2, L, (b) #9, L + perovskite.

Table I. Compositions of the equilibrium phases at 1400°C detected by EDS, wt.%

	Initial composition					Equilibrium phase compositions					
No.	TiO$_2$	SiO$_2$	CaO	MgO	Al$_2$O$_3$	Phases	TiO$_2$	SiO$_2$	CaO	MgO	Al$_2$O$_3$
#2	5.00	31.82	38.18	10.00	15.00	L	5.5 ± 0.1	34.3 ± 0.1	39.9 ± 0.05	7.4 ± 0.04	12.7 ± 0.02
#6	15.00	27.27	32.73	10.00	15.00	L	13.8 ± 0.04	32.1 ± 0.07	31.4 ± 0.1	8.2 ± 0.03	14.3 ± 0.04
						Perovskite	57.2 ± 0.6	0.1 ± 0.08	41.4 ± 0.3	0.1 ± 0.05	1.0 ± 0.1
#9	20.00	25.00	30.00	10.00	15.00	L	15.3 ± 0.1	30.9 ± 0.1	29.4 ± 0.08	8.8 ± 0.05	15.5 ± 0.03
						Perovskite	57.7 ± 0.2	0.1 ± 0.03	41.2 ± 0.2	0.1 ± 0.00	0.7 ± 0.3
#12	25.00	22.73	27.27	10.00	15.00	L	19.5 ± 0.05	29.4 ± 0.06	25.9 ± 0.1	9.1 ± 0.06	15.8 ± 0.1
						Perovskite	57.9 ± 0.20	0.0 ± 0.01	41.3 ± 0.1	0.1 ± 0.03	0.5 ± 0.01
#15	30.00	22.50	22.50	10.00	15.00	L	28.7 ± 0.08	25.8 ± 0.02	23.9 ± 0.03	7.7 ± 0.04	13.7 ± 0.05
#16	30.00	20.45	24.55	10.00	15.00	L	27.4 ± 0.07	25.3 ± 0.09	23.9 ± 0.05	8.4 ± 0.04	14.8 ± 0.05
						Perovskite	57.9 ± 0.4	0.1 ± 0.01	41.2 ± 0.01	0.1 ± 0.01	0.4 ± 0.02

Equilibria Phase Relations at 1300°C

The equilibrium phase relations at 1300°C were quite different from those at 140°C, as shown by microstructures of the equilibrium phases in Fig. 4 and the equilibrium phase compositions in Table II.

An example of a single quenched glassy phase is given by sample #1 and shown in Fig. 4a. The similar results were also found in samples #7 and #10. The liquid–perovskite two-phase equilibrium was also detected in sample #3, shown as a white phase (perovskite)and a gray matrix phase (liquid) in Fig. 4b. The same equilibrium results were also confirmed for samples #4 and #5, and a comparison of the liquid compositions for samples #3, #4, and #5 is shown in Fig. 3b, which also depicts the experimental tie lines for the liquid–perovskite two-phase equilibria.

In sample #9, the liquid–perovskite two-phase equilibrium at 1400°C was transformed into a three-phase equilibrium when the temperature was decreased to 1300°C, as shown in Fig. 4c. A new solid spinel phase (black, the contrast in BSED) was detected in the assemblage. In sample #13, another two-phase equilibrium of liquid–pseudobrookite was confirmed, see Fig. 4d, where the dark gray matrix phase is the quenched glassy liquid phase, and the light polygon-shaped gray phase is the pseudo-brookite solid solution. It has been reported[38] that pseudobrookite is a solid solution phase composed in titania ores of four end-members: MgO·2TiO$_2$, Al$_2$O$_3$·TiO$_2$, FeO·2TiO$_2$, and Ti$_3$O$_5$. In the present experimental conditions, there was no iron involved, and in air titanium existed as Ti^{4+}. Thus, in this work, the pseudobrookite phase can be simplified to
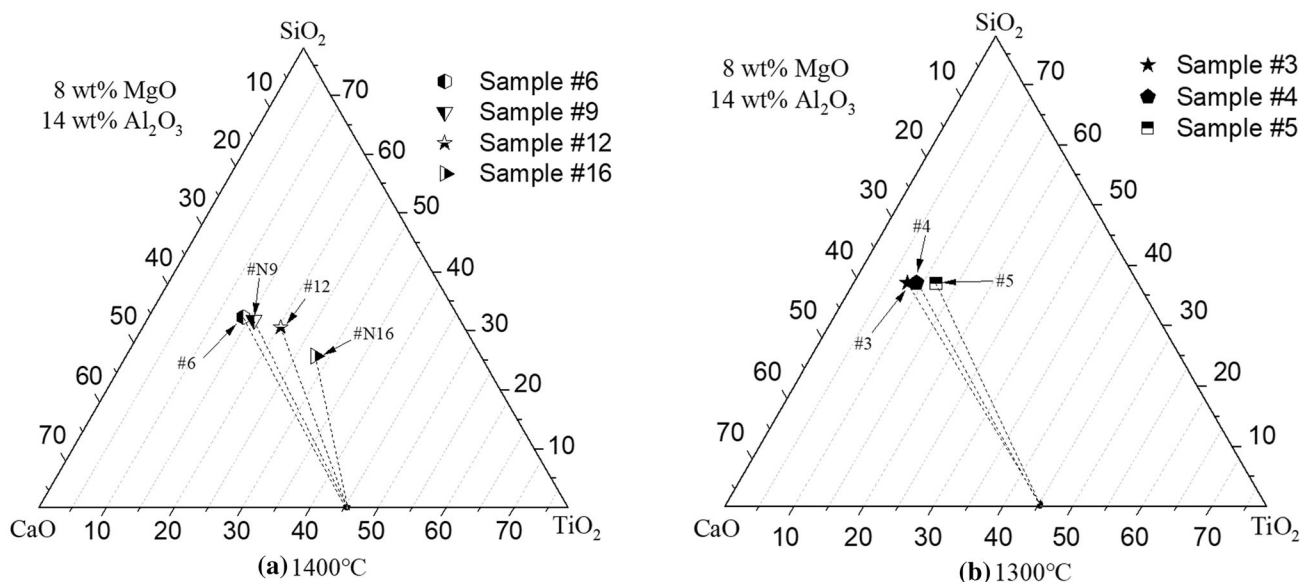
Fig. 3. Projection of tie lines for liquid-perovskite equilibrium at (a) 1400°C, and (b) 1300°C, wt.%.

as a quasibinary solution phase of $MgO \cdot 2TiO_2$-$Al_2O_3 \cdot TiO_2$.

Construction of the 1300°C and 1400°C Isotherms

Based on the experimental results and the above discussion, the 1300°C and 1400°C isotherms were constructed for the CaO-8 wt.% MgO-14 wt.% Al_2O_3-SiO_2-TiO_2 system and are presented in Fig. 5a and b. Predictions by Factsage and MTDATA thermodynamic software, as well as the experimental results from the literature,[39,40] were also superimposed on the isothermal sections. The solid lines in Fig. 5 are the experimentally determined isotherms, while the dashed lines (Fig. 5a) and dash-dot lines (Fig. 5b) are the predictions of MTDATA and Factsage, respectively.

The present experimental results generally agree well with the liquidus compositions from the literature.[39,40] It is also obvious from the comparison in Fig. 5a that both the experimental 1300°C and 1400°C isotherms agree well with the results calculated using MTDATA in the perovskite liquid oxide primary phase field. However, a great deviation exists in the pseudobrookite–liquid primary phase field. The liquidus domain of 1300°C predicted by MTDATA is much smaller than the experimental ones. In the comparison with the predictions by Factsage in Fig. 5b, a fair degree of agreement is obtained with the 1300°C and 1400°C isotherms of the liquid–perovskite equilibrium. Both the 1300°C and 1400°C isotherms calculated by Factsage have a much wider liquid phase domain compared with the experimental ones, especially when the location of the liquid–pseudobrookite equilibrium is concerned. Similar observations were also reported by Wang et al.,[28] who compared predictions by Factsage with

experimental data from different authors.[19,41,42] It was found that up to 130°C higher liquidus temperatures existed in the computational primary phase field of rutile. According to Wang et al.,[28] the main reason for the disagreement was that the properties of the primary phase fields of spinel, as well as the pseudobrookite primary phase fields, for example, were not detailed enough in the thermodynamic databases of Factsage.

From the present equilibrium results and the 1300°C and 1400°C isotherms constructed above, it can be confirmed that the compositions of industrial Ti-bearing blast furnace slags are mainly located in the perovskite primary phase field perovskite, which is the dominant titanium-containing phase in such slags. With a TiO_2 content higher than 25 wt.%, but in lower $w(CaO)/w(SiO_2)$ ratios, the primary phase may move to the spinel or pseudobrookite domains. It is, however, clear that more experimental data are needed for accurate description of the primary phase fields for these equilibrium phases.

CONCLUSION

The equilibrium phase relationships of the CaO-MgO-Al_2O_3-SiO_2-TiO_2 system at 1300°C and 1400°C, close to the 8 wt.% MgO-14 wt.% Al_2O_3 quasiternary section, were studied experimentally using a high-temperature equilibration and quenching method followed by SEM–EDS phase analysis. Equilibrium solid phases of perovskite, spinel and a pseudobrookite solid solution of $MgO \cdot 2TiO_2$ and $Al_2O_3 \cdot TiO_2$ joint were found to coexist in equilibrium with the liquid oxide. The 1300°C and 1400°C isotherms were constructed using the experimental phase composition data from the present study and the available literature. Comparisons with the
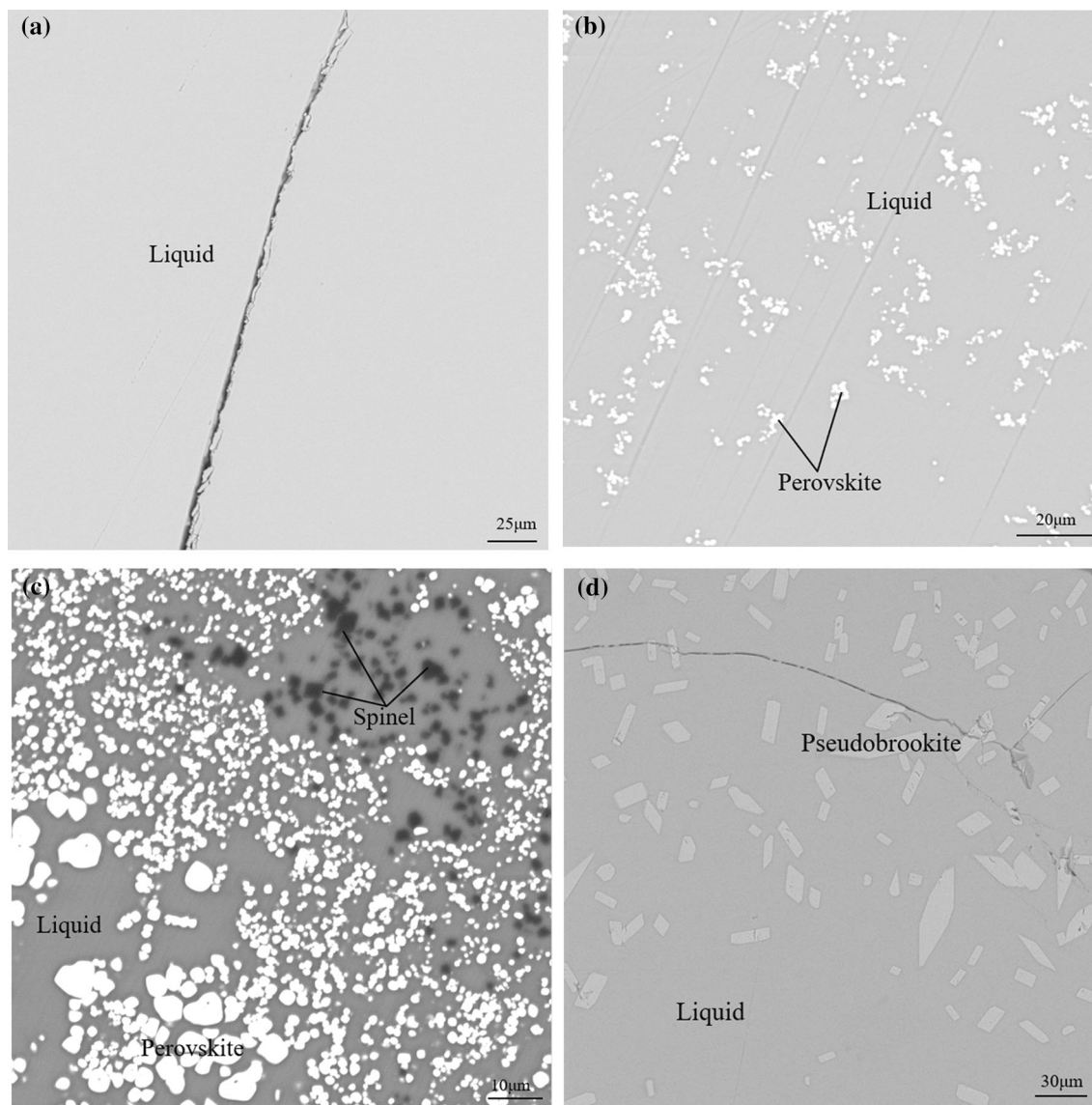
Fig. 4. SEM microscopic morphologies of equilibrium phases at 1300°C. (a) #1, L, (b) #3, L + perovskite, (c) #9, L + perovskite + spinel, (d) #13, L + pseudobrookite.

Factsage and MTDATA predictions indicated that the calculated results only agreed well in the primary phase field of perovskite, whereas there were significant deviations within the other primary phase fields in this temperature range. The results of the present work can be used for optimizing the phase descriptions and thermodynamic databases for titanium oxide slags, and also for understanding the reduction smelting processes for titano-magnetite ores.

Table II. Compositions of the equilibrium phases at 1300°C detected by EDS, wt.%

|	Initial composition					Equilibrium phase compositions					
No.	TiO$_2$	SiO$_2$	CaO	MgO	Al$_2$O$_3$	Phases	TiO$_2$	SiO$_2$	CaO	MgO	Al$_2$O$_3$
#1	5.00	35.00	35.00	10.00	15.00	L	5.1 ± 0.04	41.5 ± 0.07	33.7 ± 0.3	5.8 ± 0.1	13.6 ± 0.2
#3	10.00	32.50	32.50	10.00	15.00	L	7.7 ± 0.05	37.2 ± 0.04	33.1 ± 0.05	7.6 ± 0.04	14.1 ± 0.05
						Perovskite	56.9 ± 0.1	0.9 ± 0.02	40.6 ± 0.06	0.2 ± 0.01	1.1 ± 0.02
#4	10.00	29.55	35.45	10.00	15.00	L	9.0 ± 0.08	37.2 ± 0.2	31.9 ± 0.06	7.7 ± 0.03	13.9 ± 0.3
						Perovskite	57.5 ± 0.03	0.2 ± 0.01	41.3 ± 0.06	0.0 ± 0.00	0.8 ± 0.01
#5	15.00	30.00	30.00	10.00	15.00	L	11.5 ± 0.05	36.1 ± 0.04	28.3 ± 0.02	8.6 ± 0.05	15.2 ± 0.04
						Perovskite	57.3 ± 0.2	0.4 ± 0.01	41.0 ± 0.03	0.1 ± 0.01	0.9 ± 0.02
#6	15.00	27.27	32.73	10.00	15.00	L	16.9 ± 0.2	34.1 ± 0.3	24.5 ± 0.2	9.2 ± 0.1	15.1 ± 0.1
						Perovskite	55.7 ± 0.1	1.9 ± 0.08	40.3 ± 0.2	0.5 ± 0.02	1.4 ± 0.03
						Spinel	1.0 ± 0.02	1.8 ± 0.08	0.9 ± 0.03	26.7 ± 0.3	69.2 ± 0.2
#7	20.00	30.56	24.44	10.00	15.00	L	20.1 ± 0.06	34.0 ± 0.03	24.7 ± 0.03	7.3 ± 0.03	13.7 ± 0.04
#8	20.00	27.50	27.50	10.00	15.00	L	15.2 ± 0.2	34.5 ± 0.2	25.1 ± 0.2	9.1 ± 0.02	15.9 ± 0.07
						Perovskite	54.5 ± 0.2	2.8 ± 0.07	39.8 ± 0.10	0.8 ± 0.01	1.8 ± 0.03
						Spinel	0.9 ± 0.02	1.7 ± 0.07	0.2 ± 0.04	26.9 ± 0.05	70.0 ± 0.07
#9	20.00	25.00	30.00	10.00	15.00	L	11.9 ± 0.2	35.3 ± 0.05	29.8 ± 0.2	8.9 ± 0.2	13.9 ± 0.2
						Perovskite	57.4 ± 0.02	0.1 ± 0.01	41.6 ± 0.02	0.1 ± 0.01	0.6 ± 0.01
						Spinel	0.9 ± 0.01		0.3 ± 0.02	27.5 ± 0.09	71.0 ± 0.1
#10	25.00	27.78	22.22	10.00	15.00	L	26.1 ± 0.08	30.3 ± 0.04	23.2 ± 0.1	7.6 ± 0.05	12.7 ± 0.08
#11	25.00	25.00	25.00	10.00	15.00	L	21.5 ± 0.05	31.7 ± 0.07	22.8 ± 0.07	8.6 ± 0.02	15.1 ± 0.05
						Perovskite	57.9 ± 0.3	0.2 ± 0.02	40.8 ± 0.08	0.2 ± 0.06	0.7 ± 0.04
						Spinel	1.4 ± 0.02	1.2 ± 0.03	0.6 ± 0.01	27.0 ± 0.1	69.6 ± 0.09
#12	25.00	22.73	27.27	10.00	15.00	L	16.4 ± 0.05	34.7 ± 0.08	23.8 ± 0.3	9.6 ± 0.2	15.3 ± 0.2
						Perovskite	57.6 ± 0.03	0.2 ± 0.01	40.7 ± 0.03	0.2 ± 0.01	1.0 ± 0.02
						Spinel	1.5 ± 0.07	1.5 ± 0.03	1.0 ± 0.01	27.0 ± 0.1	68.7 ± 0.2
#13	30.00	28.13	16.88	10.00	15.00	L	28.9 ± 0.04	31.5 ± 0.1	18.9 ± 0.10	7.6 ± 0.05	12.9 ± 0.04
						Pseudobrookite	73.7 ± 0.1	1.7 ± 0.04	1.7 ± 0.02	14.8 ± 0.1	7.9 ± 0.02
#14	30.00	25.00	20.00	10.00	15.00	L	31.7 ± 0.2	25.8 ± 0.2	21.9 ± 0.2	7.5 ± 0.06	12.9 ± 0.1
						Perovskite	57.9 ± 0.01	0.0 ± 0.02	41.4 ± 0.01	0.1 ± 0.02	0.4 ± 0.01
						Spinel	1.1 ± 0.1	0.0 ± 0.09	0.2 ± 0.05	27.6 ± 0.08	70.9 ± 0.2
#16	30.00	20.45	24.55	10.00	15.00	L	25.2 ± 0.2	30.3 ± 0.2	22.1 ± 0.1	8.8 ± 0.1	13.5 ± 0.2
						Perovskite	58.4 ± 0.2	0.1 ± 0.01	40.6 ± 0.2	0.1 ± 0.01	0.6 ± 0.02
						Spinel	2.6 ± 0.01	1.9 ± 0.02	1.5 ± 0.01	25.5 ± 0.07	68.3 ± 0.1
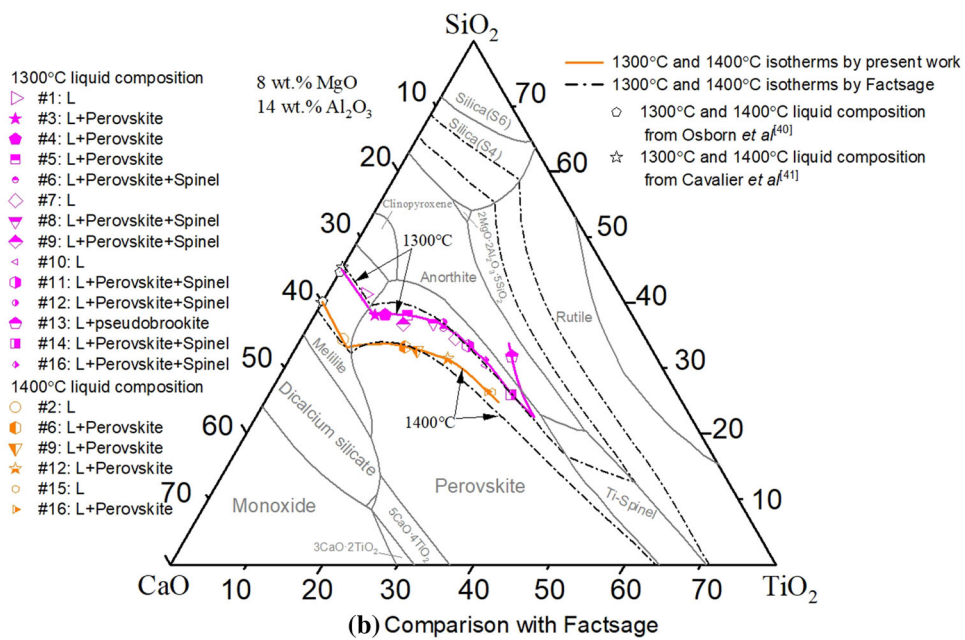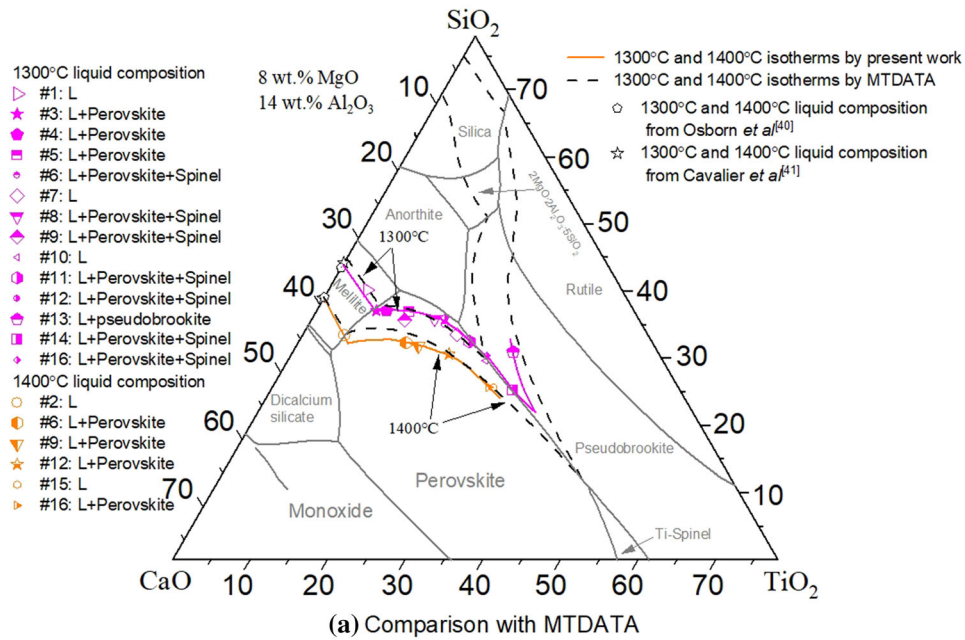
Fig. 5. Experimental and computational isotherms at 1300°C and 1400°C for the titanium-bearing slag system of this study and selected literature data, wt.%: (a) comparison with MTDATA, (b) comparison with Factsage.

need to obtain permission directly from the copyright holder. To view a copy of this licence, visit http://creativecommons.org/licenses/by/4.0/.

REFERENCES

1. B. Lin and Z. Du, *Energy Policy* 104, 285 (2017).
2. P. Jin, Z. Jiang, C. Bao, S. Hao, and X. Zhang, *Resour. Conserv. Recy.* 117, 58 (2017).
3. I. Sohn and D.J. Min, *Steel Res. Int.* 83, 611 (2012).
4. M. Hanao, T. Tanaka, M. Kawamoto, and K. Takatani, *ISIJ Int.* 47, 935 (2007).
5. Q. Zhao, C. Liu, L. Cao, M. Jiang, B. Li, H. Saxén, and R. Zevenhoven, *ISIJ Int.* 59, 583 (2019).
6. D.H. Woo, Y.B. Kang, and H.G. Lee, *Metall. Mater. Trans. B* B33, 920 (2002).
7. J. Qiu, C. Liu, Z. Liu, and Z. Yu, *Ceram. Int.* 45, 2281 (2019).
8. R.C. DeVries and E.F. Osborn, *J. Am. Ceram. Soc.* 40, 6 (1957).
9. M.R. Rao, *J. Am. Ceram. Soc.* 51, 50 (1968).
10. B.A. Vazquez, A. Caballero, and P. Pena, *J. Am. Ceram. Soc.* 88, 1949 (2005).
11. X. Ma, G. Wang, S. Wu, J. Zhu and B. Zhao, *ISIJ Int.* 55, 2310 (2015).
12. VDEh, *Slag Atlas*, 2nd ed. (Düsseldorf: Stahleisen, 1995), p. 111.
13. S. Arnout, D. Durinck, M. Guo, B. Blanpain, and P. Wollants, *J. Am. Ceram. Soc.* 91, 1237 (2008).
14. J.H. Park, I.H. Jung, and S.B. Lee, *Met. Mater. Int.* 15, 677 (2009).
15. H.C. Chuang, W.S. Hwang, and S.H. Liu, *Mater. Trans.* 50, 1448 (2009).
16. Y.H. Gao, Z.Y. Liang, Q.C. Liu, and L.T. Bian, *Asian J. Chem.* 24, 5337 (2012).
17. J. Li, Z.T. Zhang, and X.D. Wang, *Ironmak. Steelmak.* 39, 414 (2012).
18. E.F. Osborn and K.H. Gee, *Bull. Earth Min. Sci. Exp. Stn.* 85, 57 (1969).
19. J.J. Shi, L.F. Sun, J.Y. Qiu, B. Zhang, and M.F. Jiang, *J. Alloys. Compd.* 699, 193 (2017).
20. J.J. Shi, L.F. Sun, J.Y. Qiu, B. Zhang, and M.F. Jiang, *ISIJ Int.* 56, 1124 (2016).
21. L.F. Sun, J.J. Shi, Z. Yu, and M.F. Jiang, *Ceram. Internat.* 45, 481 (2019).
22. B.J. Zhao, E. Jak, and P.C. Hayes, *J. Iron Steel Res. Int.* 16, 1172 (2009).
23. Z. Wang, Q. Zhu, and H. Sun, *Metall. Mater. Trans. B* B50, 357 (2019).
24. S.S. Kim and T.H. Sanders, *J. Am. Ceram. Soc.* 82, 1901 (1999).
25. H. Mao, M. Hillert, M. Selleb, and B. Sundman, *J. Am. Ceram. Soc.* 89, 298 (2006).
26. I. Johnson and P.S. Maiya, *J. Mater. Res.* 9, 739 (1994).
27. M. Kirschen and C. DeCapitani, *J. Phase Equilibria* 20, 593 (1999).
28. S. Wang, M. Chen, Y. Guo, T. Jiang, and B. Zhao, *Calphad* 63, 77 (2018).
29. C.W. Balea, E. Bélislea, P. Chartranda, S.A. Decterova, G. Erikssonb, A.E. Gheribia, K. Hackb, I.-H. Jung, Y.B. Kang, J. Melançon, A.D. Pelton, S. Petersen, C. Robelin, J. Sangster, P. Spencer, and M.-A. Van Ende, *Calphad* 54, 35 (2016).
30. J.A. Gisby, P. Taskinen, J. Pihlasalo, Z. Li, M. Tyrer, J. Pearce, K. Avarmaa, P. Björklund, H. Davies, M. Korpi, S. Martin, L. Pesonen, and J. Robinson, *Metall. Mater. Trans. B* 48B, 91 (2017).
31. M. Chen, J.J. Shi, P. Taskinen, and A. Jokilaakso, *Ceram. Int.* (2019). https://doi.org/10.1016/j.ceramint.2019.12.170.
32. J. Shi, M. Chen, I. Santoso, L.F. Sun, M.F. Jiang, P. Taskinen, and A. Jokilaakso, *Ceram. Int.* 46, 1545 (2020).
33. L. Zhang, L.N. Zhang, M.Y. Wang, G.Q. Li, and Z.T. Sui, *J. Non-Crystall. Solids* 353, 2214 (2007).
34. Z. Wu, Z. Li, Z. Ju-hua, and F.N. Xiang, *Ind. Eng. Chem. Res.* 51, 12294 (2012).
35. S. Lyu, X. Ma, M. Chen, Z. Huang, Z. Yao, G. Wang, and B. Zhao, *Calphad* 68, 101721 (2020).
36. R.H. Davies, A.T. Dinsdale, J.A. Gisby, J.A.J. Robinson, and A.M. Martin, *Calphad* 26, 229 (2002).
37. T.I. Barry, A.T. Dinsdale, J.A. Gisby, B. Hallstedt, M. Hillert, B. Jansson, and J.R.J. Taylor, *J. Phase Equilibria* 13, 459 (1992).
38. T. Jantzen, K. Hack, E. Yazhenskikh, and M. Müller, *Calphad* 62, 187 (2018).
39. E.F. Osborn, R.C. DeVries, K.H. Gee, and H.M. Kraner, *JOM* 6, 33 (1954).
40. G. Cavalier and M. Sandrea-Deudon, *Rev. Metall.* 57, 1143 (1960).
41. J.J. Shi, L.F. Sun, J.Y. Qiu, and M.F. Jiang, *J. Alloys Compd.* 722, 25 (2017).
42. J.J. Shi, L.F. Sun, J.Y. Qiu, and M.F. Jiang, *ISIJ Int.* 58, 431 (2018).